MATERIALS SCIENCE

New power of self-assembling carbonic anhydrase inhibitor: Short peptide–constructed nanofibers inspire hypoxic cancer therapy

Jiayang Li[1]*, Kejian Shi[1]*, Zeinab Farhadi Sabet[1,2]*, Wenjiao Fu[1], Huige Zhou[1], Shaoxin Xu[1], Tao Liu[1], Min You[1], Mingjing Cao[1], Mengzhen Xu[1], Xuejing Cui[1], Bin Hu[1], Ying Liu[1], Chunying Chen[1,2]†

Carbonic anhydrase (CA) IX overexpresses exclusively on cell membranes of hypoxic tumors, regulating the acidic tumor microenvironment. Small molecules of CA inhibitor modified with short peptide successfully achieve CA IX–targeted self-assembly that localizes CA inhibitors on hypoxic cancer cell surfaces and enhances their inhibition efficacy and selectivity. CA IX–related endocytosis also promotes selective intracellular uptake of these nanofibers under hypoxia, in which nanofiber structures increase in size with decreasing pH. This effect subsequently causes intracellular acid vesicle damage and blocks protective autophagy. The versatility of tunable nanostructures responding to cell milieu impressively provokes selective toxicities and provides strategic therapy for hypoxic tumors. Moreover, in vivo tests demonstrate considerable antimetastatic and antiangiogenesis effects in breast tumors, and particularly remarkable enhancement of antitumor efficacy in doxorubicin administration. With its biocompatible components and distinctive hypoxia therapies, this nanomaterial advances current chemotherapy, providing a new direction for hypoxic cancer therapy.

INTRODUCTION

As a characteristic feature of various solid tumors, hypoxia has profound clinical significance in treatment of multidrug resistance (*1*), and metastasis (*2*, *3*). Among the large family of α-carbonic anhydrases, carbonic anhydrase (CA) IX is known as a tumor-associated enzyme (*4*), overexpressed exclusively in the hypoxic regions of various tumors, including carcinoma of the brain, neck, lung, bladder, breast, cervix, uterus, etc. (*5*). One of its main functions in solid tumor is pH regulation, which affords extracellular acidification in the tumor microenvironment, benefiting the acquisition of both chemoresistant and metastatic phenotypes in hypoxic tumor (*6*). Moreover, this transmembrane metalloenzyme simultaneously facilitates the membrane-crossing transport of the intracellular acidic products, subsequently protecting hypoxic cancer cells from acidosis during their hypoxia-induced metabolism (*7*). Current investigations have recognized that hypoxia inhibits endocytosis of tumor cells in the caveolin-1–dependent pathway. Impressively, only hypoxia-induced overexpression of CA IX may override this problem and further allow intracellular uptake of cytotoxins in certain hypoxic cancer cells (*8*). Considering the pivotal role of CA IX enzyme in hypoxic tumors (*9*), its inhibition has been validated as a diagnostic and therapeutic target for antiproliferation (*10*), antimetastasis (*11*), and antiangiogenesis (*12*) treatments in hypoxic tumors.

Traditional CA inhibitors, e.g., sulfonamides and coumarins, lack considerable selectivity for tumor-associated CA IX versus other constitutive isoforms of CA enzymes in human body (*5*). To amplify their selectivity for transmembrane isoform CA IX, investigators have attempted to modulate the chemical or physical properties of these CA inhibitors (*13*). One of the important strategies for selectively targeting CA IX is reducing their membrane permeability in cancer cells so that inhibitors preferentially bind to this cell surface isoform of CA enzymes (*14*). Among them, side-chain modification with nanoparticles has attracted considerable interest. Because of the tunable shape and size of the nanoparticles (*15*), which strongly influence process of cellular uptake (*16*), CA inhibitor–constructed nanoparticles are considered as innovative platforms to perform more specific CA IX–targeted treatments (*17*, *18*).

On the basis of the inherent biocompatibility and biodegradability, bioinspired nanostructures originated from the self-assembly of small molecules have attracted more and more attention for decades (*19*). Emerging as innovative biomaterials for increased applications in biomedicine (*20*–*22*), peptide-based self-assembles extraordinarily benefit tumor therapy due to their designs of cell milieu–triggered tunable nanostructures (*23*). For instance, the acidic pH–triggered geometrical changes of peptide-based nanostructures have been applied to stimulate tumor-targeting delivery and subsequent intracellular uptake (*24*). Schneider and colleagues (*25*) have found a new kind of intrinsically disordered peptide, which facilitates nonendosomal cell entry and thus directly delivers membrane impermeable cargo toward cell cytoplasm. Liang and colleagues (*26*) have developed an extra-/intracellular environment–differentiated self-assembly, affording two types of peptide-based nanostructures to achieve better tumor therapy. The mitochondria-targeting self-assembly performs effective organelle damages, resulting in marked cellular dysfunction in cancer (*27*). Zhao and colleagues (*28*) have developed a distinctive transformable peptide nanosystem, targeting cancer-associated fibroblasts and expeditiously delivering anticancer drugs. Moreover, a new strategy, forming pericellular nanonets through tumor microenvironment–induced self-assembly of peptides, for blocking mass exchange between cancer cells, restricting tumor cell migration (*29*), or homing theranostic agents as noninvasive implants in tumor region (*30*) has also recently emerged.

[1]CAS Key Laboratory for Biomedical Effects of Nanomaterials and Nanosafety and CAS Center for Excellence in Nanoscience, National Center for Nanoscience and Technology of China, Beijing 100190, People's Republic of China. [2]University of Chinese Academy of Sciences, Beijing 100049, People's Republic of China.
*These authors contributed equally to this work.
†Corresponding author. Email: chenchy@nanoctr.cn

As an innovative method to engineer cell surface that strongly interfere with functioning of normal membrane-related enzymes (*31*), these pericellular supramolecular nanostructures therefore present a potent strategy for altering interaction mechanisms of enzymes with cells (*32*), promoting or reducing their cellular uptakes.

Given the fact that the hypoxic cancer–associated CA IX enzyme has an extracellular active site, a self-assembly design of peptide-based CA inhibitors can be constructed to form undesirable nanostructures for cell uptake (*33*), consequently exhibiting strong potential for extracellular therapy. In addition, current studies also reveal that CA inhibitor modification with short peptides may benefit the binding efficiency of tumor-associated CA IX enzymes (*34*, *35*). With such assets, short peptide–constructed self-assembly of CA inhibitor may prospectively enhance selective therapies targeted toward extracellular membrane CA IX. Regarding the critical role of CA IX in the tumor microenvironment, pericellular self-assembly of CA inhibitor could play a promising role in hypoxic cancer cell modulations, including pH regulation, cell migration, exosome secretion, etc. The structure-tunable designs responding to cell milieu may create opportunities for creating additional intracellular damage during CA IX–regulated endocytosis under hypoxia. Simply modified with short peptides, this smart design of traditional drug-constructing nanostructures may benefit traditional therapy not only by achieving more precise drug delivery but also undergoing innovative therapeutic mechanism.

RESULTS

Molecular design

MDA-MB-231, known as triple-negative breast cancer cells, express high levels of CA IX when they have 100% growth confluence or are cultured under hypoxic condition. Here, we design a novel small molecule based on a traditional CA inhibitor (Fig. 1A), which may elevate its inhibition efficacy and selectivity to CA IX–overexpressed hypoxic cancer cell (MDA-MB-231) by cooperating with a self-assembled peptide motif. As shown in Fig. 1B, a commercially available CA inhibitor, 4-(2-aminoethyl) benzenesulfonamide (ABS), has been chosen with limited selectivity to CA IX inhibition. After conjugating ABS with a well-established self-assembled motif [2-naphthaleneacetic acid-(D)-Phe-(D)-Phe-(D)-Lys-OH (N-pep)] (*36*), i.e., a hydrophilic short peptide sequence [(D)-Phe-(D)-Phe-(D)-Lys] and a hydrophobic naphthalene head [2-(naphthalen-2-yl)acetic acid], we obtain a self-assembled small-molecule of N-pepABS, endowed with the following new therapeutic biofunctions: (i) achieve CA IX–targeted self-assembly of this peptide-conjugated CA inhibitor on the surface of hypoxic cancer cell membrane; (ii) concentrate CA inhibitors toward transmembrane CA IX enzymes and afford enhanced inhibition efficacy, which not only interrupt their regulation of tumor microenvironment pH but also attenuate cancer cell immigration; (iii) selectively induce CA IX–regulated endocytosis of nanofibers in hypoxic cancer cell, which further performs structure upgrade of these nanofibers; and (iv) advance inhibitions of hypoxic cancer cell growth through subsequent intracellular damages of lysosomes and blockages of their protective autophagy activities. Meanwhile, we also have developed another short peptide–based small molecule of (D)-Phe-(D)-Phe-(D)-Lys-benzenesulfonamide (pepABS), which contains exactly the same sequence of hydrophilic peptide in N-pepABS. Without a hydrophobic naphthalene head, pepABS displays as poor a self-assembling ability as small-molecule ABS. Lacking enough selective CA IX inhibition and relevant pericellular therapeutic functions, pepABS and ABS, as negative controls, may advance us to better understand the important role of the self-assembled nanofiber-like structures of N-pepABS during a hypoxic cancer therapy.

Hypoxic cancer cell–targeted self-assembly

In vitro experiments exhibit good self-assembly abilities for both N-pepABS and N-pep. As shown in Fig. 1C, 7.5 mg of N-pepABS was dissolved in 1 ml of double-distilled H_2O (ddH_2O) and formed transparent hydrogel [0.75 weight % (wt %)] under the well-known tumor microenvironment pH (6.5). Transmission electron microscope (TEM) images reveal the uniform nanofibers of N-pepABS, which afford network structure with an average width of 13 ± 3 nm (Fig. 1D). The oscillatory rheology data prove that 0.75 wt % of N-pepABS forms stable hydrogel materials at pH 6.5 (fig. S1). With obviously higher storage moduli (G') than its loss moduli (G''), the hydrogel performs viscoelastic properties of a solid-like material, which are independent to frequency sweep. As a self-assembling motif control, we also prepared N-pep to study its gelation property under the same pH condition, which forms stable hydrogel (0.75 wt %) with a nanofiber average width of 14 ± 2 nm. As pH value decreased to 5.5 (the pH mimicking intracellular acid vesicles), N-pepABS forms a more opaque and stable hydrogel with stronger G' value in rheology, while N-pep turns to be a solution due to increasing protonation effects of its ε-ammonium group (NH_3^+). Here, we also investigate the self-assembly properties of pepABS and ABS. Figure 1C shows the optical images of pepABS and ABS solutions (0.75 wt %). Under pH 6.5 and even pH 5.5, ABS still performs as transparent solution, while pepABS starts to precipitate. We thus use these two compounds as negative controls for their poor self-assembly abilities.

Although both N-pepABS and N-pep exhibit promising self-assembly abilities under weak acidic condition (pH 6.5), they perform differently on the surface of hypoxic MDA-MB-231 cells due to their opposite binding effects toward CA IX. We have treated hypoxic MDA-MB-231 cells with 500 μM N-pepABS and N-pep have been for 24 hours, respectively, and compared them with medium control group. Then, we observe the cell surfaces using an environment scanning electron microscope. As shown in Fig. 1E, N-pepABS–treated group exhibits obvious nanofibers and afford dense network structures that cover the cell surface, while both medium control and N-pep groups show normal intact cell membrane images. In addition, the N-pepABS treatment after 48 hours also exhibits some gel-like materials on the bottom of the culture dish (Fig. 2A). All of these appearances come along with higher mRNA and protein levels of CA IX (Fig. 2C), indicating their CA IX enzyme dependences. However, we did not observe considerable evidence of self-assembly in N-pep and control groups, which convinces us that the CA inhibitor part of the molecule in N-pepABS does perform recognition function and actualizes the CA IX–targeted self-assembly of N-pepABS on surface of hypoxic cell membrane.

Inhibition of CA IX–regulated cancer cell behaviors

On the basis of these results, we also detected biological functions of our self-assembled small molecule. One of the most important functions of CA IX enzymes is their ability to regulate pH. Under hypoxic conditions, CA IX enzyme decreases the extracellular pH of cancer cells to pH 6.5, while maintaining intracellular pH at around pH 7.4 (*6*, *7*). This important function not only helps hypoxic cancer cell survival under glycolysis metabolism but also

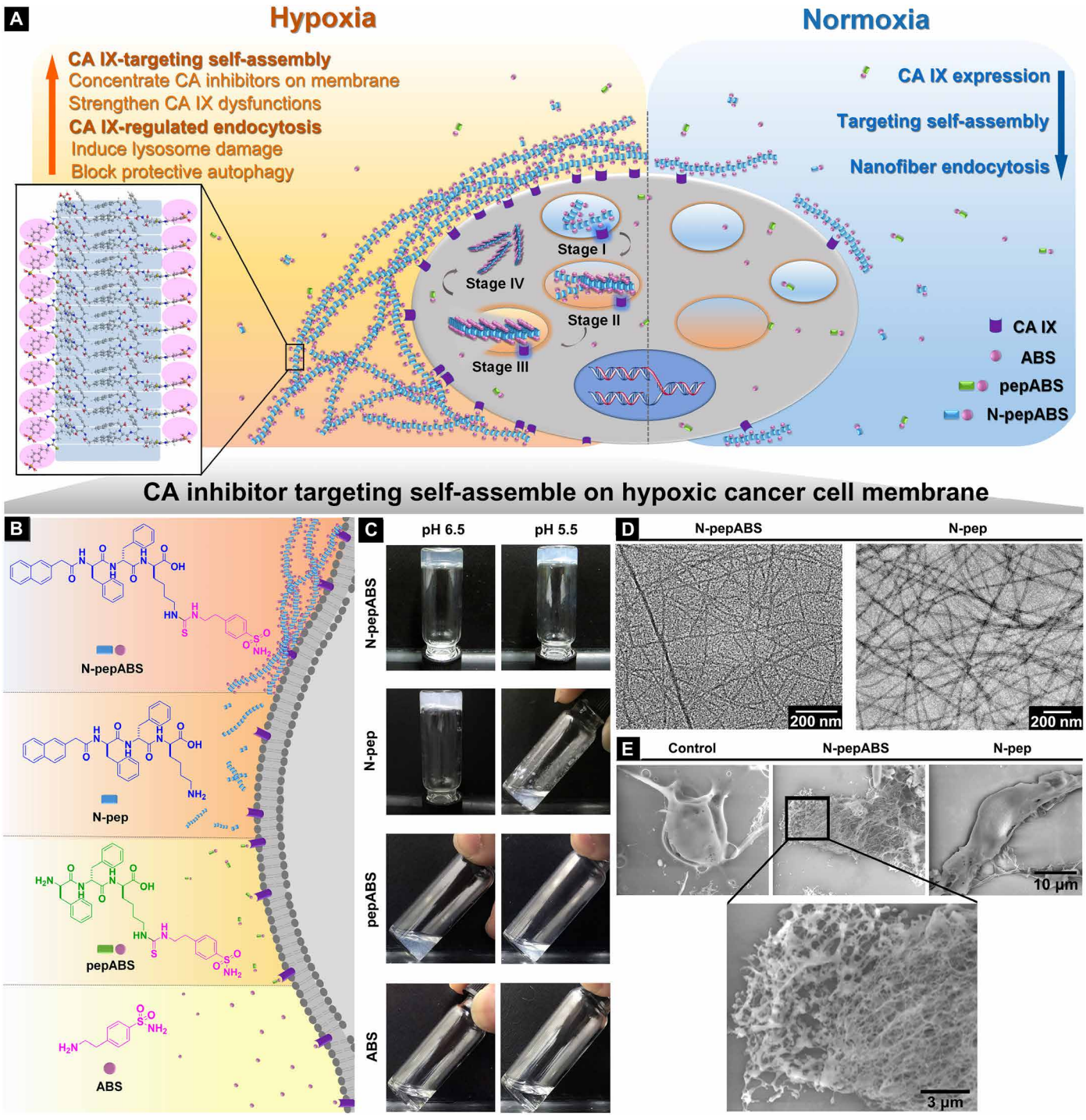

Fig. 1. Molecular design of self-assembled CA IX inhibitors and their hypoxic cancer cell–targeted self-assembly. (**A**) Depending on overexpression of CA IX enzymes of hypoxic cancer cells, small molecules of N-pepABS achieve CA IX–targeted self-assembly, which concentrate CA IX inhibitors on hypoxic cancer cell membrane and subsequently interrupt the normal activities of hypoxic cancer cells. In addition, these N-pepABS–based nanofibers undergo CA IX–regulated endocytosis, promoting intracellular uptakes of the self-assembled nanofibers under hypoxia. During the process of internalization (stages I to IV), N-pepABS–based nanofibers may convert to much bigger bunches of nanofiber that pierce intracellular acid vesicles, therefore introducing highly selective toxicities for hypoxic cancer cells. (**B**) The chemical structures of self-assembled CA IX inhibitors. (**C**) In vitro gelation performance of N-pepABS, N-pep, pepABS, and ABS at pH 6.5 or pH 5.5. (**D**) Transmission electron microscope (TEM) images of hydrogels formed by 0.75 wt % of N-pepABS and N-pep at pH 6.5. (**E**) Environment scanning electron microscope images of MDA-MB-231 cells after 24-hour incubation with 500 μM medium control, N-pepABS, or N-pep under hypoxia condition (1.0% of O_2) (Photo credit: Chunying Chen, The National Center for Nanoscience and Technology of China).

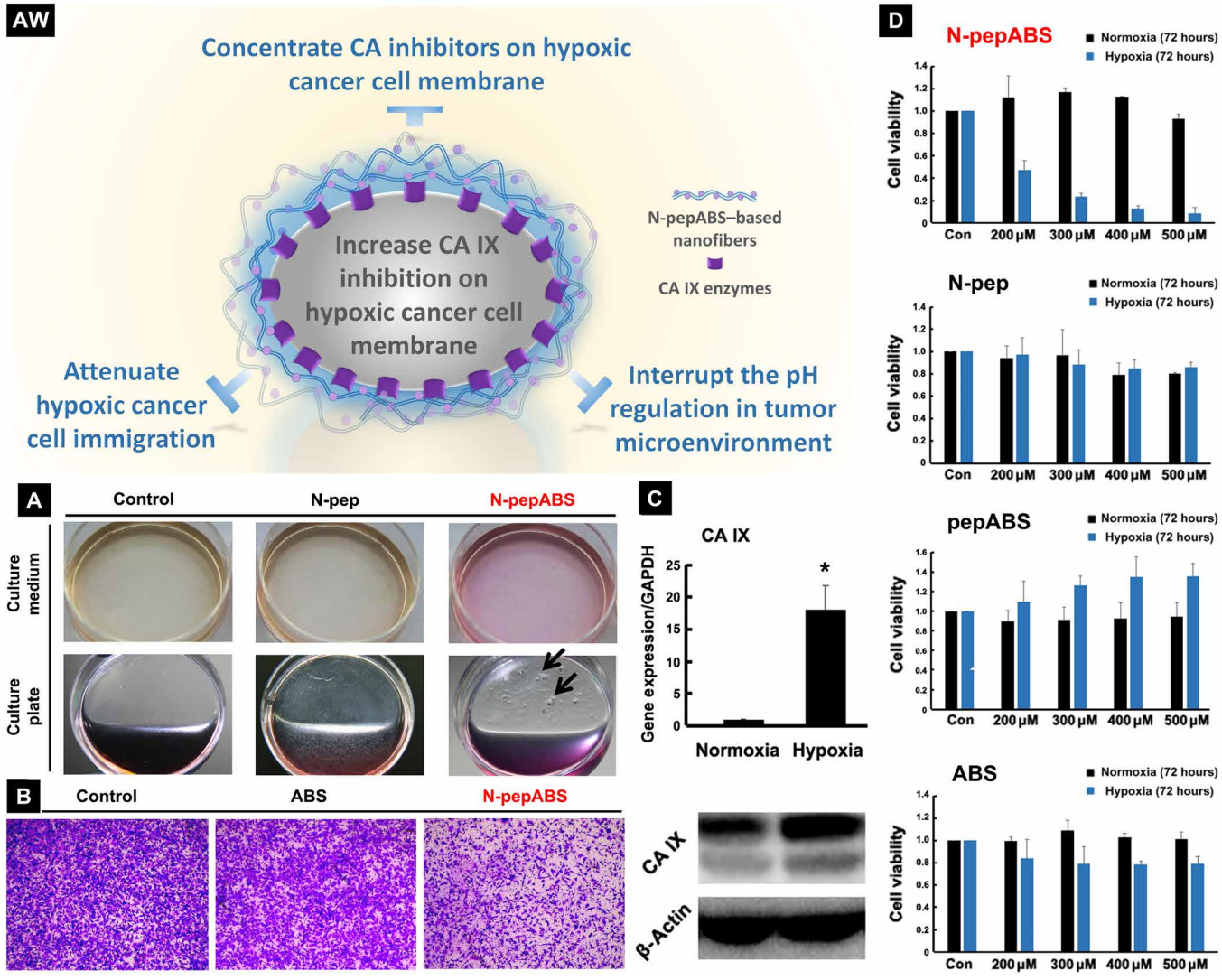

Fig. 2. Nanofibers inhibit CA IX–associated cancer cell behaviors. (**AW**) Self-assembled nanofibers may concentrate CA inhibitors on the hypoxic cancer cell membrane, enhancing their inhibitory effect. (**A**) The alterations of extracellular culture medium after 48-hour treatment of 500 μM N-pepABS or N-pep for MDA-MB-231 cells under hypoxia, with the appearance of gel-like materials (black arrows) on the bottom of culture plate. (**B**) Transwell data of MDA-MB-231 cells treated with 200 μM N-pepABS, ABS, and solvent control for 24 hours under hypoxia, followed by another 10-hour migration in the upper chamber. (**C**) The mRNA and protein expression level of CA IX after cells incubated for 48 hours. GAPDH, glyceraldehyde-3-phosphate dehydrogenase. (**D**) Cell proliferation of MDA-MB-231 with treatment of N-pepABS, N-pep, pepABS, or ABS, respectively, for 72 hours under both hypoxia (sky blue) and normoxia (black). The bar image was represented as means ± SD, while $^*P < 0.05$ was thought as significant difference (Photo credit: Chunying Chen, The National Center for Nanoscience and Technology of China).

facilitates their migration behaviors. Figure 2A shows the considerable color change of the culture medium in N-pep and control groups. This pale yellow color of medium indicates a pH decrease after 48-hour incubation under hypoxia (1.0% O_2). However, when we treat the hypoxic MDA-MB-231 and HeLa cells with a small molecule of N-pepABS (500 μM) for 48 hours, the culture medium stays pink, which implies the possibility of dysfunction in CA IX enzymes (fig. S2). Notably, this type of alkalization in cancer microenvironment could also frustrate the anaerobic metabolism in cancer cells, which is necessary for cell survival under hypoxia. In addition, we also detect metastasis behaviors of hypoxic cancer cells via transwell assay. Under hypoxic condition (1.0% O_2), we treat MDA-MB-231 cells with 200 μM N-pepABS for 24 hours, which has no obvious toxicity to hypoxic MDA-MB-231 cells yet (fig. S2). Then, we let them migrate from the upper side to the lower side of the film in the upper chamber for another 10 hours. Figure 2B exhibits that N-pepABS treatment implements the strongest effect on inhibiting tumor cells migration, even compared with the commercially available CA inhibitor ABS itself. This interesting phenomenon should be originated from the CA IX–targeted self-assembly of N-pepABS, which concentrates the CA inhibitors on cell membrane and may benefit their binding efficacies. These not only attenuate the activities of transmembrane CA IX enzymes but also restrict normal movements for hypoxic cancer cells. A similar appearance has also been observed in N-pepABS–treated HeLa cells (fig. S2). Therefore, our peptide-conjugated CA inhibitor N-pepABS performs advanced inhibition efficacies for CA IX.

Selective inhibition of hypoxic cancer cell growth

Although the self-assembly of N-pepABS on MDA-MB-231 cell surface successfully inhibited hypoxic cancer cell migration in vitro.

However, how it influences the cancer cell growth under hypoxia is still unknown. Therefore, we have also assessed cell viabilities of MDA-MB-231 cells after 72 hours of exposure with N-pepABS, N-pep, pepABS, or ABS, respectively. As shown in Fig. 2D, cholecystokinin-8 (CCK-8) assays demonstrate that our molecules inhibit hypoxic MDA-MB-231 cells in a dose-dependent manner. Among these four compounds, only N-pepABS performs a marked inhibition effect for hypoxic cancer cell after 72 hours. Instead, similar treatments with N-pep, pepABS, and CA IX inhibitor ABS as negative controls exhibit limited toxicities to hypoxic cancer cells due to their poor targeting or self-assembling abilities. This selective killing effect of N-pepABS has also been observed in CA IX overexpressing HeLa cells, and these interesting results confirm that modifying a normal CA inhibitor with self-assembled peptides can largely enhance its therapeutic effects toward CA IX–overexpressed cancer cell. To be noticed, N-pepABS treatment affords not only higher toxicity than ABS does but also higher selectivity for hypoxic cancer cell therapy. N-pepABS treatment presents very limited toxicity under normoxia, although it also slightly induces nanofibers on normoxic cell surface due to its certain level of CA IX expression (fig. S2). This paradoxical phenomenon incites us into deeper mechanism study for the hypoxic cancer cell growth inhibition by CA IX–targeted self-assembly of N-pepABS.

CA IX regulated the endocytosis of nanofibers

It has been recently demonstrated that CA IX can be recycled between the cell surface and intracellular vesicle system, while CA IX antibody initiates endocytosis just through its interaction with CA IX (*37*). Moreover, recent studies have also found that hypoxia inhibits endocytosis of tumor cells in a caveolin-1–dependent pathway, while CA IX–related stimulation can override this problem and further allow CA IX–targeting cytotoxin delivery into hypoxic cells (*8*). Inspired by this novel function of CA IX enzymes, we speculate that N-pepABS–based nanofibers may interact with CA IX and further promoted CA IX–related endocytosis, which might be responsible for the selective growth inhibitory effect of this molecule. Several experiments have been carried out to explore the exact biological mechanisms behind this phenomenon. Indicated with CA IX antibodies in green color, MDA-MB-231 cells show a higher level of CA IX enzyme expression under hypoxia than normoxia (Fig. 3A). Meanwhile, Early Endosome Antigen 1 (EEA1) proteins, known as marker of early endosome, are shown in red to visualize the process of hypoxic endocytosis of MDA-MB-231 cells. Figure 3A illuminates that MDA-MB-231 cells with medium treatments (−) undergo a relative low level of endocytosis and EEA1 aggregation under hypoxia. However, N-pepABS treatment (+) for 24 hours distinctly stimulates more aggregations for EEA1 under hypoxia, many of which are colocalized with CA IX (white arrows). Meanwhile, we have also used the bar graph of Pearson's *r* value fold change to evaluate the colocalization of EEA1 with CA IX (fig. S3B). This result implies that N-pepABS treatment under hypoxia does impressively induce endocytosis, which should be associated with the regulation of CA IX enzymes. Because endocytosis of cargoes would undergo early endosomes, late endosomes, and lysosomes orderly, the damage of intracellular acid vesicles and subsequent inhibition of hypoxic tumor cells growth caused by N-pepABS treatments should also be associated with this CA IX–related endocytosis. CA IX–regulated endocytosis of N-pepABS–based nanofibers presents strong selectivity to hypoxia. Different from small molecules of CA IX inhibitor ABS, the self-assembly of N-pepABS affords nanofibers on cell membrane, which may hardly diffuse inside the cell. Instead, the intracellular uptake of these N-pepABS–based nanofibers needs to undergo energy-consuming endocytosis. Lacking high-level expression of CA IX enzymes, MDA-MB-231 cells under normoxia perform limited activities of CA IX–regulated endocytosis of N-pepABS–based nanofibers. As shown in fig. S3, no obvious increase in EEA1 signal appears in N-pepABS treatment group under normoxia, and its merged image also exhibits few colocations with CA IX. However, treatment with ABS itself under normoxia does show some colocations of CA IX and EEA1 enzymes. The colocalization of EEA1 with CA IX has also been evaluated with the bar graph of Pearson's *r* value fold change. Therefore, N-pepABS treatment exhibits more selective intracellular uptake for hypoxic MDA-MB-231 cells.

We have also monitored the subsequent processing of CA IX–regulated endocytosis of N-pepABS nanofibers. Lysosomal-associated membrane protein 1—partially maintaining lysosomal pH, integrity, and catabolism—has been stained after treating with 500 μM N-pepABS for 48 hours. Only under hypoxia, Fig. 3B exhibits plenty of hollow spheres, which indicates that cytosolic vesicles were undergoing swelling process. Flow cytometry assay confirms that N-pepABS treatment evidently damages intracellular acid vesicles (e.g., late endosomes and lysosomes) under hypoxia. As shown in Fig. 3C, the fluorescence intensity of intracellular lysosensors in hypoxic MDA-MB-231 cells is decreased after the treatment of 500 μM N-pepABS for 48 hours, followed by another 40-min incubation with 2.5 μM lysosensor. After DND-189 staining, Fig. 3D directly illuminates the decrease in intracellular acid vesicles (white arrows) under hypoxia, subsequently causing fluorescence attenuation in flow cytometry assay. Once CA IX enzyme has been knocked down, the decrease in lysosome acidity is partly reversed (fig. S4). Thereafter, we further collect cancer cell lysates and their membrane residues, respectively, after different treatments. Concentration of N-pepABS in each sample has been analyzed via ultrahigh-performance liquid chromatography (UHPLC). As shown in fig. S4 (C and D), both intracellular and extracellular accumulation of N-pepABS under hypoxia exhibit remarkable attenuations ($^*P < 0.05$), along with down-regulation of CA IX expression. Consistent with previous cell viability results, N-pepABS treatment under hypoxia, therefore, may induce obvious damages for intracellular acid vesicles, which should also contribute to its inhibition selectivity. Moreover, this result might indicate distinct intracellular uptakes of N-pepABS–based nanofibers in hypoxic MDA-MB-231 cells, which should depend on the CA IX–regulated endocytosis. All of the results confirm that N-pepABS selectively destroys intracellular acid vesicles in hypoxic MDA-MB-231 cells through CA IX–related endocytosis, resulting in increased inhibition of cell growth under hypoxia.

Characterization of nanofiber internalization

Here, we have also characterized nanofiber internalization and captured the morphology of N-pepABS–based nanofibers during CA IX–regulated endocytosis. Accompanied with CA IX–regulated endocytosis process, the environmental pH value may decrease from 6.5 to 5.0, consequently affording different sizes of N-pepABS–based nanofibers. Figure 4 (A to D) reveals this pH-triggered secondary self-assembly of these uniform nanofibers, which is also consistent with their rheology performances. Unlike the thin and flexible nanofibers formed under tumor microenvironment pH (6.5) (Fig. 4A), N-pepABS has much thicker and longer nanofibers of N-pepABS under pH 5.5, composing of network structures entangled by uniform nanofibers

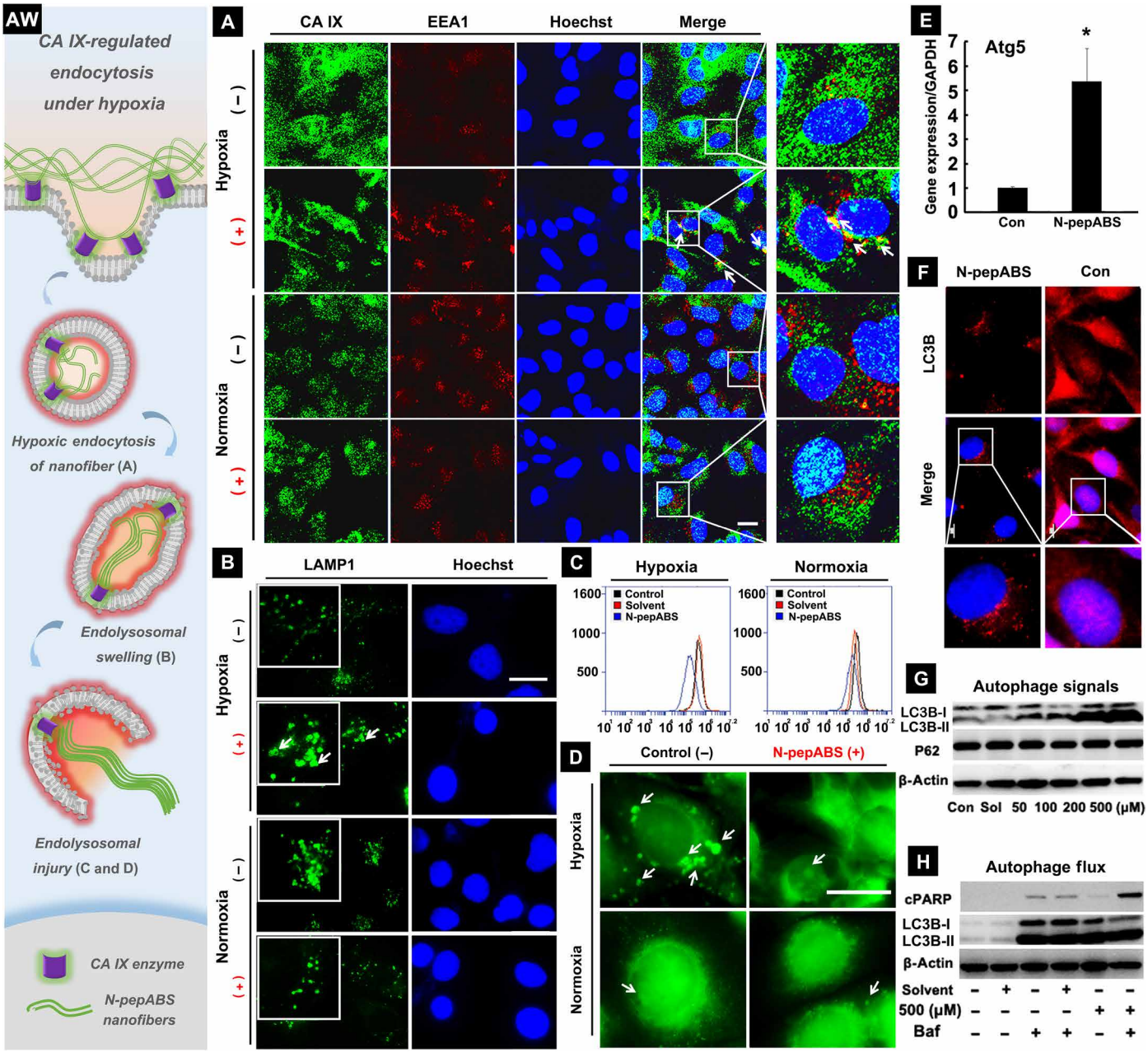

Fig. 3. Nanofibers promote CA IX–regulated endocytosis under hypoxia. (**AW**) Artwork here illuminates the whole process of CA IX-regulated endocytosis for nanofibers under hypoxia. (**A**) CA IX–regulated endocytosis of N-pepABS nanofibers has appeared under hypoxia after 24-hour treatment of 500 μM N-pepABS (+) or medium control (–). Scale bar, 20 μm. We further observe subsequent (**B**) endolysosomal swelling and (**C** and **D**) intracellular acid vesicles injuries after 48-hour treatment of 500 μM N-pepABS under hypoxia. Scale bars, 20 μm. Then, blockage of protective autophagy has been detected after 48-hour treatment of 500 μM N-pepABS. (**E**) Ratio of mRNA levels of Atg5/GADPH, with the bar image represented as means ± SD, while $^*P < 0.05$ was thought as significant difference. (**F**) Fluorescence images of autophagosome accumulation in the cytoplasm of hypoxic cancer cells. Scale bars, 20 μm. LC3B, light chain 3B. (**G**) Western blot assays of autophagy-related signals in MDA-MB-231 cells and their (**H**) autophagy flux study with 1-hour pretreatment of 10 nM bafilomycin A1 (Baf). cPARP, cleaved poly(adenosine diphosphate–ribose) polymerase.

with a diameter of 24 ± 5 nm (Fig. 4B). The acidity also triggers the secondary self-assembly of these uniform nanofibers (Fig. 4C), affording much larger bunches of fibers. These nanofibers should lastly bundle up with a diameter of 280 ± 45 nm and a length of larger than 10 μm (Fig. 4D). Further information of circular dichroism (CD), ultraviolet (UV)/visible spectroscopy, and fluorescence spectroscopy have been studied to support this conformation transitions via chiral self-assembly under acidic condition. As shown in fig. S1C, the self-assembly of N-pepABS hydrogels would afford intense peaks at around 260 to 330 nm, which should neither belong to nature peptide structures nor monomer's chirality (diluted solutions of N-pepABS at pH 9.0 or in methanol). Instead, the positive Cotton effect for the peak at 255 nm of N-pepABS hydrogel (pH 7.0) should be originated from their strong π-π interactions between aromatic

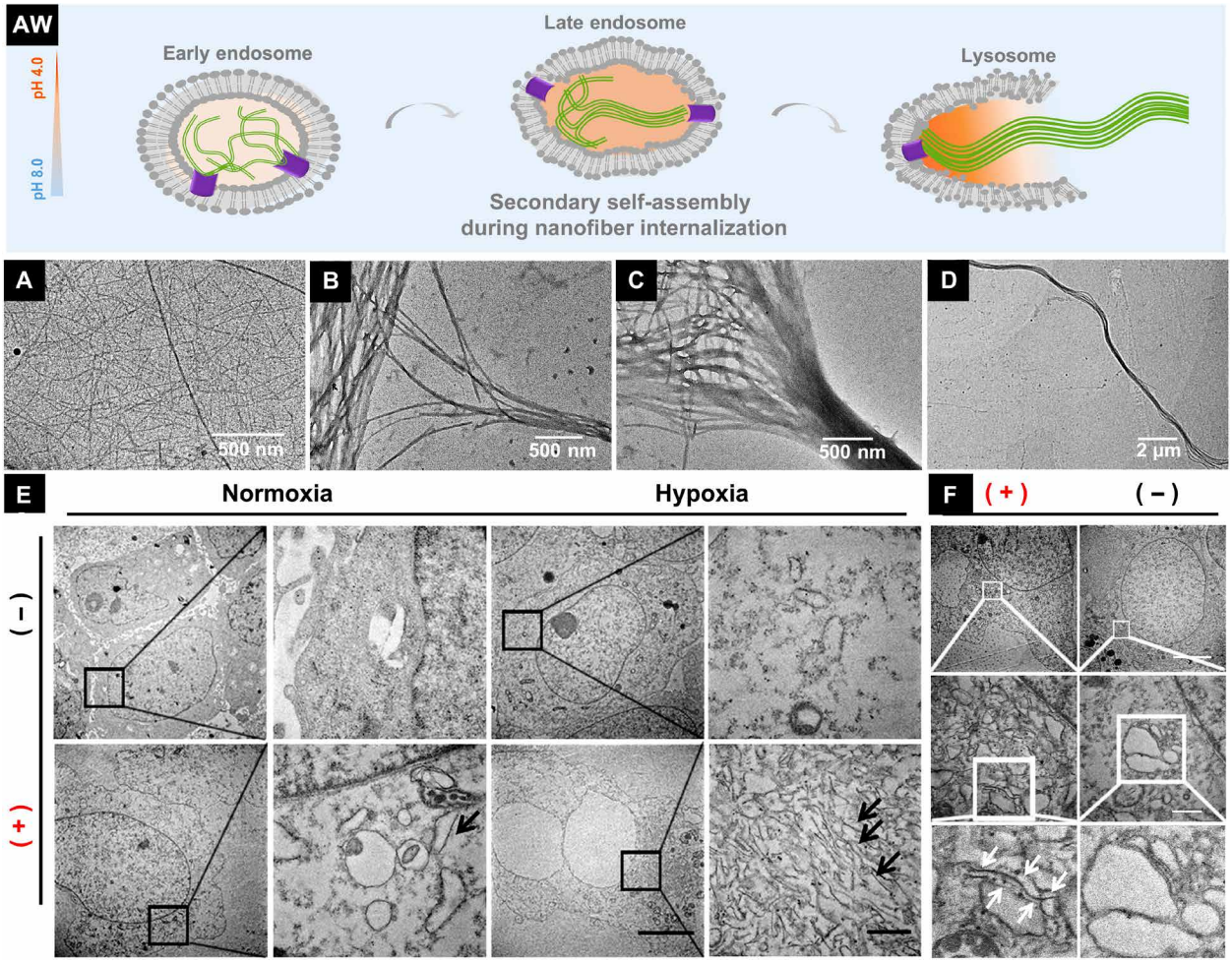

Fig. 4. CA IX–induced nanofiber internalizations in hypoxic cancer cells. (**AW**) Hypothesis of structure upgrades during CA IX-induced nanofiber internalization. TEM images of nanofibers formed by 0.75 wt % of N-pepABS at (**A**) pH 6.5 or (**B** to **D**) pH 5.5. TEM images of nanofibers (**E**) dissociatively appearing in the cytoplasm (black arrows) and (**F**) destroying monolayer vesicles (white arrows) of hypoxic MDA-MB-231 cells, after 48-hour treatment of 500 mM N-pepABS. Scale bars, 5 μm (E) and 500 nm (F).

rings of D-phenylalanine and naphthalene head via J-type aggregation (*38*, *39*). The considerable red shift of UV absorption (fig. S1D) and CD signals may confirm the J-aggregation of N-pepABS during their chiral self-assembly. As pH value decreased to 5.0, however, the positive peak at 255 nm has disappeared in N-pepABS hydrogel. Instead, a new peak at 300 nm has unexpectedly emerged with intense negative Cotton effect. Both the changes of peak position and direction in CD spectra indicate the occurrence of conformation transitions. They might be raised from a secondary J-aggregation (stronger red shifting and increased fluorescence intensity), at the same time, affording an inverse direction helical self-assembly under acidic condition (*40*). Therefore, we can not only use the flexible nanofibers of N-pepABS to cover and interrupt hypoxic cancer cell membrane functions around neutral pH but also use nanofiber bunches to pierce and destroy intracellular acid vesicles with decreasing pH during CA IX–related endocytosis. This useful upgrade of the nanostructures responding to cell milieu in N-pepABS treatment should provide versatile and strategic hypoxic cancer cells therapy.

We further implement cell experiments to study the CA IX–related internalization of N-pepABS–based nanofibers by TEM images. As shown in Fig. 4E, medium control groups provide the morphology of healthy cancer cells. However, after treating MDA-MB-231 cells with 500 μM N-pepABS for 48 hours, we directly observe the straight, rigid, and smooth fiber-like structures in the cytoplasm, which exhibit distinctly different structures to other organelle in normal cancer cells. These newly emerging structures should belong to N-pepABS–based nanofibers that destroy the monolayer vesicles under hypoxia condition at the late period of N-pepABS treatment. Figure 4F also provides the image of pierced vesicles by nanofibers under hypoxia, predicting the process of transporting pericellular nanofibers into cytoplasm. Therefore, after the intracellular uptake of N-pepABS through endocytosis, nanofibers will be transferred into late endosomes and lysosomes, whose acidic environments may further promote the formation of bigger bunches of nanofibers. As a result, these nanofibers therefore pierce and then escape from the vesicles. Furthermore, the TEM image of cells with N-pepABS treatment under hypoxia presents a large area of nanofibers in cytoplasm, while normoxia only got a few of them (fig. S3C). Considering the special staining process in TEM preparation, extracellular information would be partially muted. Therefore, TEM experiments should be more suitable and reliable to visualize intracellular CA IX–related performances, which again convinces

us that the N-pepABS treatment performs high selectivity for hypoxic tumor cells.

Blockage of protective autophagy

Transferring damaged proteins and organelles to the late endosome and lysosome for degradation, autophagy in tumor cells often performs self-contradictory functions. It may normally induce type II programmed cell death; however, it also protects and repairs cancer cells in some way. Therefore, investigations of the mechanism for autophagy initiation and function are necessary for cancer therapy. Here, we monitor the activities of autophagy with the treatment of N-pepABS under hypoxia. By examining the expression of autophagy initiation markers Autophagy related 5 (Atg5), we observe that the mRNA level ratio of Atg5/glyceraldehyde-3-phosphate dehydrogenase has been up-regulated (Fig. 3E). Illuminated with microtubule-associated protein 1A/1B light chain 3B (LC3B) antibody, Fig. 3F exhibits that the dispersed cytosolic form of LC3B (LC3B-I) has been converted to autophagosome membrane localized form (LC3B-II), further confirming autophagosome accumulation in the cytoplasm of hypoxic tumor cells. In addition, P62, one of the common degradation substrate of autophagy, is supposed to present decreasing signals along with the autophagosome accumulation. However, Fig. 3G does not show any notable down-regulation of P62, suggesting that autophagy flux might be blocked.

Moreover, bafilomycin A1 (Baf), an inhibitor of H^+–adenosine triphosphatase, has been recruited to inhibit the fusion process of lysosome and autophagosome, which should help us better understand the mechanism of autophagy flux blockage. After pretreatment with 10 nM Baf for 1 hour and after N-pepABS was given for another 48 hours, LC3B-II, known as both initiation marker and degradation substrate of autophagy, does not exhibit extra increase compared to the N-pepABS treatment without Baf (Fig. 3H). This not only confirms the blockage of autophagy under hypoxic N-pepABS treatment but also implies that its blocking mechanism should be associated with relevant lysosome damages. On the contrary, this combined treatment of N-pepABS and Baf under normoxia obviously incites an extra increase in LC3B-II, demonstrating limited lysosome damages that appeared in previous normoxic treatments (fig. S5). In addition, Fig. 3H also shows the alteration of cleaved poly(adenosine diphosphate–ribose) polymerase from a Western blot experiment, indicating that autophagy in N-pepABS–treated hypoxic cells has protective effects. So far, we have found that self-assembled N-pepABS can destroy intracellular vesicles, such as late endosome and lysosome, and further blocked autophagy flux, which has a protective role in hypoxic MDA-MB-231 cells. All of these events would interfere with the balance of intracellular homeostasis and affect cell growth on hypoxic tumor cells, thereafter performing selectively inhibitory.

Antihypoxia performance in human breast tumor model

So far, in vitro cell experiments have already revealed the marked potential of N-pepABS for selectively inhibiting hypoxic MDA-MB-231 cancer cells. Encouraged by their underlying mechanism studies, we here perform animal experiments to fully prove the key concepts of this design in vivo. A breast cancer xenograft–bearing nude mouse model was adopted to analyze the antihypoxic cancer cell effect of N-pepABS, in which 10^7 MDA-MB-231 cells were injected subcutaneously. We first let mice bear tumors with average volume up to 250 mm^3, ensuring the formation of a hypoxic region inside tumor tissue, then gave the treatments of N-pepABS, pepABS, N-pep, ABS, and solvent control via intratumoral injections every 4 days (1 mM, 10 μl) (fig. S6). After totally treating the mice for 32 days, we collected their tumor tissues and specifically analyzed the hypoxic area through immunofluorescence assay (Fig. 5, A and B). Both CA IX and hypoxia-inducible factor–1α (HIF-1α), as characteristic biomarkers, overexpress in the region far from blood vessels of solid tumor in solvent control group (stained in red). However, only N-pepABS treatment notably weakens the signals of HIF-1α and CA IX, implying the success of attenuating hypoxia condition inside solid tumor. Notably, none of the treatments with N-pep, pepABS, and ABS exhibit comparable efficacies of this hypoxia attenuation. Moreover, an exclusive increase in autophagosome accumulation, as dot-like structures of LC3B, appeared in the N-pepABS–treated group (Fig. 5C). According to our previous in vitro results, this distinguishing inhibition efficacy of N-pepABS in hypoxia may possibly benefit from its mechanism of the formation and endocytosis of its self-assembled nanofiber structure. Figure 5D confirms that cancer cell proliferation in N-pepABS–treated group is much more inactive than other control groups, which is also consistent with our previous in vitro cell experiments. Together with these data, N-pepABS treatment does perform considerable therapeutic effects for hypoxic tumor in vivo with statistical significance ($^{**}P < 0.01$) toward solvent control group (fig. S6). Meanwhile, the N-pepABS treatment group exhibits no obvious abnormality in both mice weights and their organs structures, ensuring its biocompatibility for in vivo applications.

Antimetastasis effects in murine breast tumor model

Because of the critical role of CA IX enzyme in hypoxic tumor microenvironment, CA IX inhibitors not only perform as antiproliferation drugs but also afford antimetastasis (*11*) and antiangiogenesis (*12*) functions in hypoxic tumors. Our previous in vitro immigration cell experiments have already shown some related behaviors. To further extend the potential antimetastasis applications of N-pepABS, herein, we focus on murine 4T1 breast cancer cell, famous for its highly tumorigenic and invasive characteristics that help 4T1 mammary carcinoma spontaneously metastasize from the primary tumor to various distant sites. In vitro cell experiment has confirmed that N-pepABS treatment can afford apparent antiproliferation effects on 4T1 cancer cell under hypoxia (0.1% O_2 concentration) after 24 hours, while ABS does not (Fig. 5E). Then, we used a homologous mouse model to investigate tumor growth and metastasis alterations in vivo.

After the subcutaneous injections of 10^5 4T1 cancer cells, we allowed healthy BALB/c mice to bear tumors with average size of around 100 mm^3 before any treatment. Next, we applied N-pepABS treatment (1 mM, 10 μl) intratumorally every 2 days. After 21 days of treatment, N-pepABS efficiently decreases the tumor volume and weight with a statistical significance (Fig. 5F). We further confirmed the antihypoxia performance of N-pepABS on 4T1 mammary carcinoma through flow cytometry. As shown in Fig. 5G, CA IX expression was detected by flow cytometry in three randomized tumor tissues from both groups (fig. S7), and statistical analysis provided quantitative evidence that N-pepABS treatment should also attenuate hypoxia condition of 4T1 breast tumor. N-pepABS treatment does show remarkable antimetastasis efficacy in this animal model. As shown in Fig. 5H, we randomly pick up three mice from each group and then carefully observe and analyze the organ structure of their lung tissues by hematoxylin and eosin staining experiment. Tumor lesions detected in each lobi pulmonis are pointed out by black arrows.

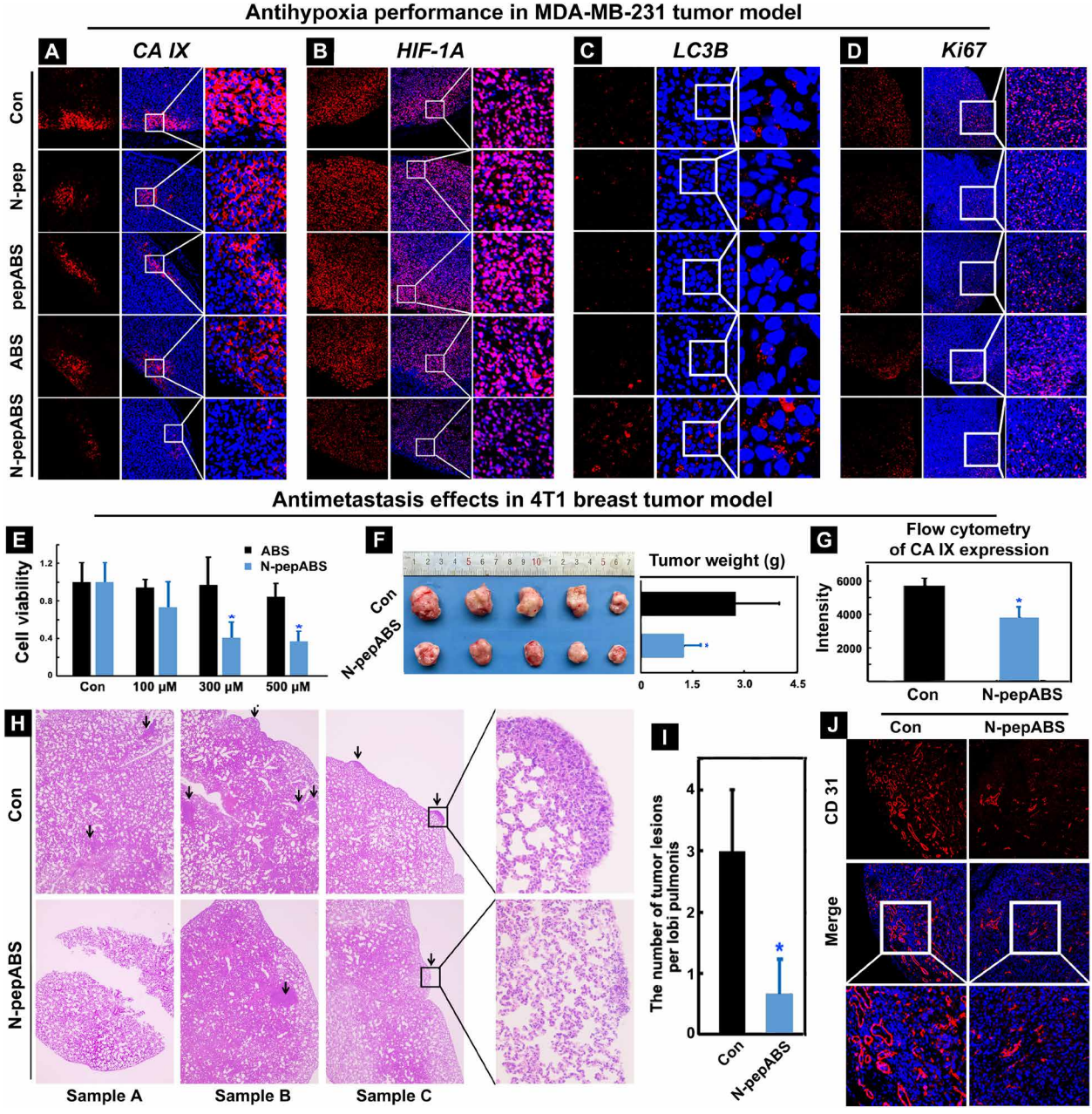

Fig. 5. Antihypoxic and antimetastasis performance of N-pepABS treatment in tumor models. Immunofluorescence images of expression alterations on (**A**) CA IX, (**B**) HIF-1α, (**C**) LC3B, and (**D**) Ki67 after treatments of phosphate-buffered saline (PBS) control, N-pep, pepABS, ABS, and N-pepABS. Inhibition of tumor growth and metastasis in 4T1 tumor model: (**E**) N-pepABS performs in vitro inhibitory effects on hypoxic 4T1 cell growth; (**F**) N-pepABS treatment apparently inhibits tumor growth and decreases tumor weight of 4T1 cancer. The bar graph was represented as means ± SD, while $^*P < 0.05$ was thought as significant difference ($n = 5$), using two-tailed t tests. (**G**) Statistical analysis of flow cytometry for CA IX expression in tumor tissues after N-pepABS treatment. The bar graph was represented as means ± SD, while $^*P < 0.05$ was thought as significant difference ($n = 3$), using two-tailed t tests. (**H**) Hematoxylin and eosin staining images of lung tissues with metastasis of 4T1 tumor cells from six different samples and (**I**) its statistical analysis of the number of tumor lesions per lobi pulmonis. The bar graph was represented as means ± SD, $^*P < 0.05$ was thought as significant difference ($n = 5$), using two-tailed t tests. (**J**) Immunofluorescence images of endothelial marker CD31, indicating blood vessel variation after N-pepABS treatment. (Photo credit: Chunying Chen, The National Center for Nanoscience and Technology of China).

Therefore, we statistically analyze the number of lung metastases in Fig. 5I, directly proving the remarkably antimetastasis function of N-pepABS. After detecting endothelial marker CD31 in the tumor tissues, we further find the antiangiogenesis efficacy of N-pepABS treatment. Immunofluorescence images of CD31 visualize the intact structure of tumor vessels in solvent control group, which has become dissociative and muted with N-pepABS treatment (Fig. 5J). This phenomenon not only supports the antimetastasis results of N-pepABS but also suggests the potential application of N-pepABS in antiangiogenesis.

Anti–CA IX treatment advances conventional chemotherapy

Hypoxia has been considered as a key issue for carcinoma progression, metastatic dissemination, and multidrug resistance occurrence in clinic. CA IX, exclusively overexpressed in the hypoxic regions of various tumors, performs as a pH regulator of tumor microenvironment and benefits the acquisition of both chemoresistant and metastatic phenotypes in solid tumor. Up to now, robust evidences convinced us that N-pepABS treatment will effectively attenuate the hypoxia region inside solid tumor through CA IX inhibition, consequently influencing tumor proliferation, metastasis, and angiogenesis. However, how does this design potentially help the conventional treatment in clinic? Here, we develop the combined treatment of N-pepABS with doxorubicin (Dox) as one example of the worldwide chemotherapeutic drugs in clinic.

We built up a cancer xenograft–bearing nude mouse model, in which nude BALB/c mice received a subcutaneous injection of 10^7 MDA-MB-231 cells and then bore tumors with average sizes larger than 100 mm^3 before any treatment. As shown in Fig. 6A, we then give the mice relatively low dosages of Dox administration intravenously (2.0 mg/kg, every 4 days), which exhibits limited suppression of tumor growth. N-pepABS treatment was simultaneously applied to mice intratumorally (1 mM, 10 μl, every 2 days), and the model was treated for 24 days to monitor the tumor growth and tissue pathology. On the basis of Fig. 6B, Dox administration does not seem to perform any effective therapy during the first 2 weeks of treatment, while N-pepABS treatment alone has some effects on retarding tumor growth. However, the combined use of N-pepABS treatment and Dox has accomplished a marked decrease in tumor volume, and this antitumor effect has sustained for the whole therapeutic period. This suggests that N-pepABS treatment can effectively sensitize tumors to Dox administration and consequently expedite conventional chemotherapy. Figure 6 (B and C) confirms the strongest antitumor efficacy of the combined treatment with N-pepABS and Dox, which obviously decreases the weight and volume of tumors after 24 days. Moreover, this combined treatment does exhibit much more serious necrotic regions (Fig. 6E) and less cell proliferations (Fig. 6F) inside their tumor tissues than other treated groups. Spontaneously, Fig. 6D evidently reveals that a lower level of CA IX expression has emerged from this combined treatment, through running Western blot assay of whole tumor tissues. Then, their antiangiogenesis performance concerning CA IX has also been detected via immunofluorescence staining. Both treatment groups involving N-pepABS do disrupt the intact blood vessels inside tumor tissues (Fig. 6G), somehow predicting the underlying mechanism of the enhanced antitumor efficacy. In addition, we evaluated toxicity effects of the combined treatment. First of all, no mouse died during the whole therapeutic period with combined treatment. After being compared with the control group, the combined use of N-pepABS and Dox does not apparently decrease the body weight of mice. The blood biochemical indexes (such as alanine aminotransferase, aspartate transaminase, and creatinine) further reflect that there are no obvious severe injuries of liver and kidney after the combined treatment of N-pepABS and Dox (fig. S8). As a whole, once we destroyed the hypoxic microenvironment of solid tumors through N-pepABS treatment, Dox treatment, even in relatively low dosage, may unexpectedly perform remarkable antitumor performance.

DISCUSSION

Accompanied by the rapid proliferation of tumor mass, hypoxia areas perform profound clinical significance in carcinoma progression and metastatic dissemination. These poorly perfused hypoxic areas not only distinctively increase the difficulties for drugs diffusion inside the tumor sites but also protect cancer stem cells, which facilitate cancer cell survivals during the traditional radio- or chemotherapies for tumor. However, current applications of hypoxic tumor therapies will be limited to their biosafety issues, penetration problems, materials stabilities, and so on. As a hypoxia-induced transmembrane enzyme, CA IX exclusively provides targets for hypoxic cancer theranostics. Taking advantage of the extracellular active site in CA IX enzyme, we have modified CA inhibitors with D version of amino acids and consequently developed short peptide–constructed self-assembled nanofibers of N-pepABS. Successfully achieving CA IX–targeted self-assembly on the cancer cell surface under hypoxia, nanofibers of CA inhibitor exhibit enhancing inhibition efficacies toward CA IX due to their longer extracellular retention time and more concentrated ligand-receptor binding. Moreover, CA IX enzyme may selectively initialize the endocytosis of these nanofiber materials, thereafter causing intracellular damage and protective autophagy blockage for hypoxic cancer cells. Taking advantages of their pericellular self-assembled performances, peptide-based CA inhibitors substantially provoke the inhibition efficacy toward membrane-localized CA IX under hypoxia.

Encouraged by these convincing in vitro phenomena and their interesting mechanisms, we have further explored the potential applications of our design from different aspects in vivo. First of all, their antihypoxia performances have been investigated through various methods and tools in vivo, such as immunofluorescence images, flow cytometry, and Western blots. Supported by these semiquantitative results, our design of self-assembled CA inhibitor has accomplished a distinguished inhibition efficacy in hypoxia via CA IX attenuation. Thereafter, we concern the CA IX–associated tumor metastasis and angiogenesis in 4T1 mammary carcinoma model, which are also notably inhibited by the treatment of N-pepABS. Dox administration, as one example of popular conventional chemotherapy, has achieved marked advances with the assist of N-pepABS treatment. Without the protection of hypoxic microenvironment, solid tumors seem to be more sensitive and intolerant to Dox administration. As we know, Dox, nowadays, is still facing the challenges for its adverse effects, such as cardiotoxicity, anaphylaxis, dyspigmentation, treatment-related leukemia, etc. (*41*). Long-term medication in chemotherapy could be dangerous and painful for patients, also raising the risk of drug resistance occurrence. Therefore, cancer interventional therapy has attracted more and more attention on its amazing effects of adjunctive therapy and pain relief. It provides locoregional treatments, such as endovascular embolization, local ablation, and topical remedy, which have been recently applied in esophageal cancer, colorectal cancer, lung cancer, and primary liver cancer (*42*, *43*). Considering the pivotal roles of CA IX enzyme in clinic, this hypoxia attenuation treatment via intratumoral therapy of self-assembled CA inhibitor should be an excellent choice for cancer interventional therapy. It not only inhibits CA IX–associated tumor angiogenesis but also effectively depresses those hypoxia areas without vascular transport of oxygen and nutrition. Benefiting from its biocompatible components and distinguished hypoxia therapies, this self-assembled CA inhibitor could be a safe and convenient material that advances and facilitates current chemotherapy.

Last but not least, modification of anticancer drugs with self-assembled short peptide provides us with more options of therapeutic

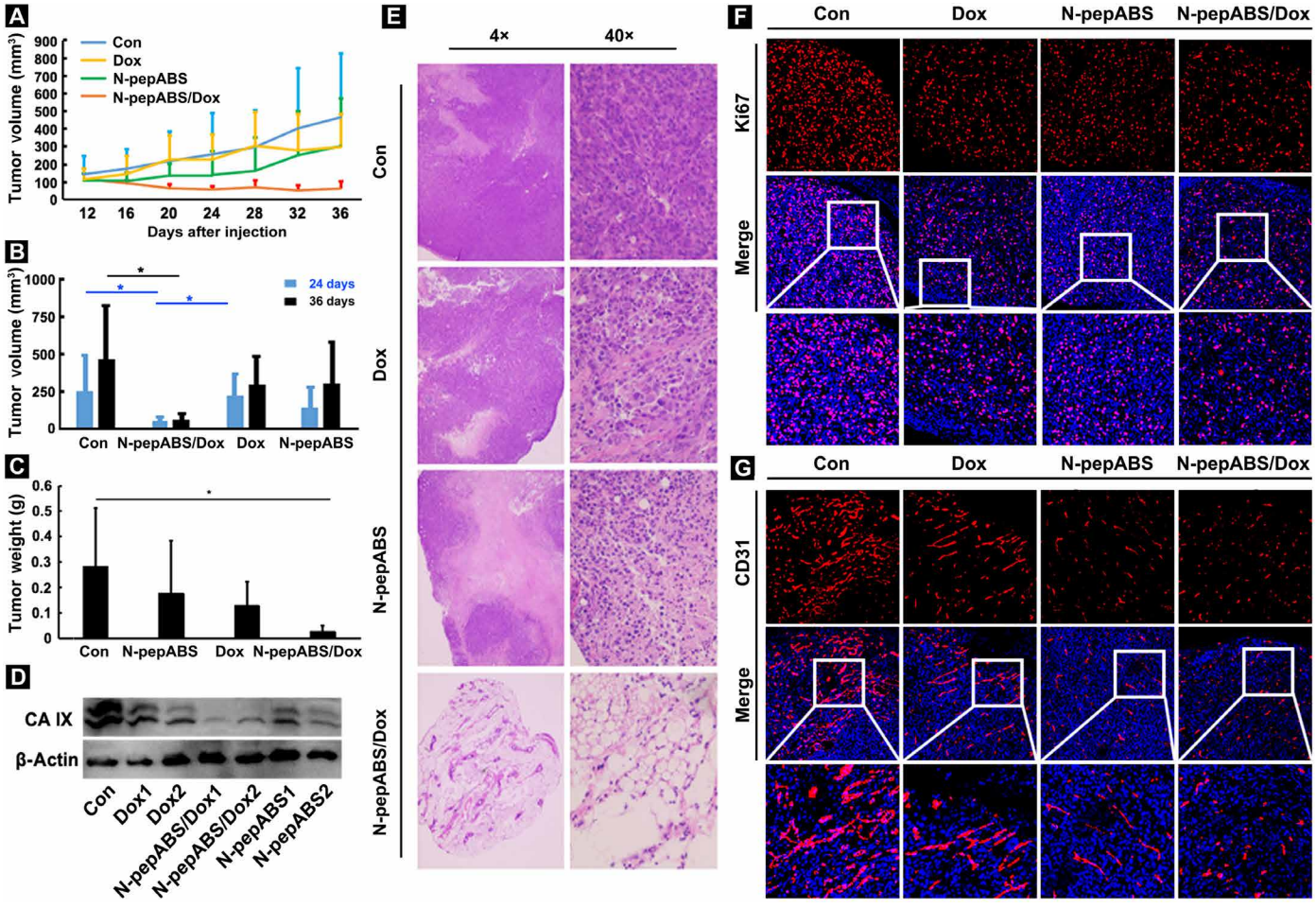

Fig. 6. The combined therapeutic efficacy of N-pepABS and low dose of Dox on MDA-MB-231 xenografts. (**A** to **D**)Tumor growth was apparently inhibited after the combination use of N-pepABS and Dox. Their volumes and weights were compared and statistically analyzed with different treatment exposures. The bar graph was represented as means ± SD, while $*P < 0.05$ was thought as significant difference ($n = 6$), performing nonparametric tests. (**E**) Necrotic regions were observed by hematoxylin and eosin staining experiments with different treatment exposures. (**F**) Western blots assays of the expression of CA IX in tumor tissues. Immunofluorescence images of (**G**) Ki67 illuminated cell proliferation attenuation, and (**H**) CD31 indicated blood vessel variation with different treatment exposures.

tools via their target-specific nanostructures. Facing challenges of large investment, long cycle, and high risks, innovative drug R&D of small-molecule compounds has entered a dead end for a time. However, drug repurposing arose as hope for drug R&D in recent years. Unlike traditional drug development, this R&D strategy can shorten clinical trial time, reduce costs, increase success rate, and effectively solve various key problems of traditional innovative drug development. Many traditional medicines—such as the anti-inflammatory drug aspirin, the alcohol-abuse drug Antabuse, the antidiabetic drug metformin, etc.—have recently been found to have completely new mechanisms and have shown unexpected performance in anticancer treatment. Inspired with drug repurposing strategy, here, we exploit the new power of traditional CA inhibitor with its self-assembled nanostructure. This work presents an excellent example that uses several amino acids to facilitate the therapeutic efficacy of traditional drugs (*34*, *35*), which should be relatively easy to approach for drug manufacture. It enables the existing traditional drugs to afford nanostructures through simple and cost-effective amino acid modifications, thereby achieving an innovative drug treatment mechanism, which consequently improve the existing clinical drug treatment. Different from current nanomedicine, which undergoes complicated and costly manufacture and has increasing safety issues as well, this smart design of traditional drug-constructing nanostructures provides a new direction for innovative drug research and development.

MATERIALS AND METHODS

Experimental materials and instruments

All of the solvents and chemical reagents were used as received from the commercial sources without further purification, unless otherwise noted. Flash chromatography was performed on silica gel (200 to 300 mesh). Analytical thin-layer chromatography was performed using silica gel 60 F-254 and analyzed by short-wave UV illumination. Hydrophilic products were purified with Waters Delta 600 high-performance liquid chromatography (HPLC) system, which was equipped with an XTerra C18 RP column and an in-line diode array UV detector. ^{1}H nuclear magnetic resonance (NMR) spectra were

obtained on Varian Unity INOVA 400. Chemical shifts are reported in δ (parts per million). Coupling constants are reported in hertz with multiplicities denoted as s (singlet), d (doublet), t (triplet), q (quartet), p (pen-tet), m (multiplet), and br (broad). TEM images were taken on Morgagni 268 TEM. The HeLa cell line (CCL2) was purchased from the American Type Culture Collection. All of the media were purchased from Invitrogen. Cytotoxicity tests were measured using DTX 880 multimode detector. The Baf (ab120497) was purchased from Abcam. The antibodies that were used for Western blotting or indirect immunofluorescence experiment, such as anti-LC3B (3868S), were purchased from Cell Signaling Technology, and CD81 (EXOAB-CD81A-1) and CD63 (EXOAB-CD63A-1) antibodies were obtained from System Biosciences, whereas anti-EEA1 (ab70521) and anti–CA IX (ab184006) antibodies were obtained from Abcam. The DyLight 488–conjugated anti-rabbit (E032220-01) and DyLight 594–conjugated anti-mouse (E032410-01) antibodies were purchased from EarthOx. The benzenesulfonamide (CA inhibitor) was purchased from Biomol, which should be relatively easy to approach for drug manufacture.

Synthesis of isothiocyanate-benzensulfonamide

ABS (0.5 mmol) was dissolved in 1 ml of *N*,*N*′-dimethylformamide (DMF), and triethylamine (3 mmol) was added into the above solution. 1,1′-thiocarbonyldiimidazole (1 mmol) was dissolved in 1.5 ml of DMF at 50°C and added dropwise to the above solution. The solution was continuously stirred at room temperature for 30 min and then quenched by ddH_2O. The product was first extracted with ethyl acetate and then purified by silica gel chromatography (ethyl acetate–hexane). ^{1}H NMR [400 MHz, dimethyl sulfoxide (DMSO)-d_6]: δ 7.79 (d, J = 7.8 Hz, 2H), 7.49 (d, J = 7.8 Hz, 2H), 7.35 (s, 2H), 3.96 (t, 2H), and 3.04 (t, 2H).

Synthesis of N-pep

The peptide hydrogelator was prepared by standard solid-phase peptide synthesis (SPPS), in which 2-chlorotrityl chloride resin (1.10 mmol/g) and Fmoc-protected amino acids with side chains protected by *tert*-butoxycarbonyl group [Fmoc-D-Lys-(Boc)-OH] were used. The resin was swelled by bubbling with nitrogen gas in dry dichloromethane (DCM) for 30 min and then was washed three times with 5 ml of dry DMF. After that first amino acid [Fmoc-D-Lys-(Boc)-OH] was added and reacted with resin at its C terminus by bubbling the resin in a DMF solution of Fmoc-protected amino acid (2 equivalent) and 1 ml of *N*,*N*-diisopropylethylamine (DIPEA) for 40 min, followed by washing the resin with 5 ml of DMF three times. Blocking solution (16:3:1 of DCM/methanol/DIPEA) was then added to resin to quench the unreacted sites in resin and bubbled twice for 10 min. The protected Fmoc group was cleaved from the resin by adding 5 ml of 20% (v/v) piperidine in DMF and bubbling for 30 min, followed by washing the resin in DMF five times. Then, Fmoc-protected amino acid (Fmoc-D-Phe-OH, 2 equivalent) was dissolved in DMF and conjugated to the free amino group on the resin, using DIPEA (1 ml)/*O*-benzotriazole-*N*,*N*,*N*′,*N*′-tetramethyl-uroniumhexafluoro-phosphate (2 equivalent). These conjugation and deprotection steps were repeated to prolong the peptide chain, which were according to standard Fmoc SPPS protocol. After each step, the resin was washed three times with 5 ml of DMF. In the final step, the resin was washed with DMF (5 ml, 5×), DCM (5 ml, 50×), methanol (5 ml, 5×), and hexane (5 ml, 5×), and then, the peptide was cleavaged from resin by adding 10 ml of trifluoroacetic acid (TFA) and bubbling for 2 hours. The product was collected by the precipitation in ether and further purified with reverse-phase HPLC. ^{1}H NMR (400 MHz, DMSO-d_6): δ 8.26 (d, J = 8.4 Hz, 1H), 8.09 (d, J = 8.1 Hz, 1H), 7.85 (d, J = 7.4 Hz, 1H), 7.78 (d, J = 7.5 Hz, 1H), 7.74 (d, J = 8.4 Hz, 1H), 7.58 (s, 1H), 7.51 to 7.42 (m, 2H), 7.29 to 7.10 (m, 10H), 4.60 to 4.54 (m, 2H), 4.54 to 4.45 (m, 1H), 4.20 (dd, 1H), 3.53 (dd, J = 35.9, 14.0 Hz, 2H), 3.08 to 3.03 (m, 2H), 2.95 to 2.79 (m, 2H), 2.69 (dd, J = 13.4, 10.3 Hz, 1H), 2.54 (s, 2H), and 1.33 to 1.62 (m, 6H).

Synthesis of pepABS

To synthesize pepABS, Fmoc-(D)-Phe-(D)-Phe-(D)-Lys-OH was first gained by SPPS. Then, pure Fmoc-(D)-Phe-(D)-Phe-(D)-Lys-OH (0.2 mmol) was added to a mixture of methanol (4 ml) and ddH_2O (1 ml), followed by adding 1 M NaOH to adjust the pH value to 8. Isothiocyanate-benzensulfonamide (iABS) (0.22 mmol) was dissolved in methanol (1 ml) and added to above solution. The mixture was stirred overnight at room temperature. After purification by HPLC, dry powder of Fmoc-(D)-Phe-(D)-Phe-(D)-Lys-(benzenesulfonamide)-OH (0.1 mmol) was collected and then dissolved in 20% (v/v) piperidine in DMF (2 ml) and reacted for 30 min. The resulting crude products were purified by reverse-phase HPLC to gain white powder. ^{1}H NMR (400 MHz, DMSO-d_6): δ 8.48 (d, J = 7.7 Hz, 1H), 8.01 (d, J = 5.3 Hz, 3H), 7.76 (d, J = 8.3 Hz, 2H), 7.50 (s, 2H), 7.42 (d, 2H), 7.39 to 7.17 (m, 10H), 4.67 (t, J = 8.8, 4.3 Hz, 1H), 4.22 (t, J = 8.3, 5.0 Hz, 1H), 4.01 (s, 1H), 3.20 to 3.03 (m, 2H), 2.98 to 2.78 (m, 4H), 2.6 (s,2H), and 1.80 to 1.32 (m, 6H).

2-Naphthaleneacetic acid-(D)-Phe-(D)-Phe-(D)-Lys-(benzenesulfonamide)-OH

N-pep (0.3 mmol) was added to a mixture of methanol (6 ml) and ddH_2O (1 ml), followed by adding 1 M NaOH to adjust the pH value to 8, and iABS (0.33 mmol) was dissolved in methanol (1 ml) and added to the solution. The mixture was stirred overnight at room temperature. The resulted crude product was purified by reverse-phase HPLC. ^{1}H NMR (400 MHz, DMSO-d_6): δ 8.25 (d, J = 8.1 Hz, 1H), 8.13 (d, J = 8.3 Hz, 1H), 7.85 (d, J = 7.4 Hz, 1H), 7.80 to 7.76 (m, 1H), 7.75 (d, J = 2.9 Hz, 2H), 7.73 (d, J = 3.5 Hz, 2H), 7.58 (s, 1H), 7.50 to 7.44 (m, 2H), 7.43 (d, 2H), 7.30 to 7.12 (m, 10H), 4.61 to 4.55 (m, 2H), 4.54 to 4.46 (m, 1H), 4.20 (dd, 1H), 3.59 (s, 2H), 3.53 (dd, J = 35.9, 14.0 Hz, 2H), 3.08 to 3.03 (m, 2H), 2.95 to 2.79 (m, 2H), 2.69 (dd, J = 13.4, 10.3 Hz, 1H), and 1.33 to 1.64 (m, 6H). Mass spectometry (electrospray ionization) (mass/charge ratio): C45H51N6O7S2 calculated 850.32; found 851.33 $[M + 1]^+$.

General procedures for hydrogel preparation

A 0.75 wt % solution of N-pepABS was prepared by dissolving 7.5 mg of N-pepABS in 1 ml of ddH_2O and adjusting the pH value around 10 with 1 M NaOH. It was sonicated to make a clear solution and monitored by pH paper, and then, the value of pH was decreased to 6.5 slowly by adding 1 M HCl and subsequently formed hydrogel. To see the difference of nanofiber morphology and hydrogel strength, another fraction of hydrogel was prepared in a similar way but with a final pH value of 5.5. The similar procedure was followed for the preparations of pepABS, ABS, and N-pep for testing their gelation abilities.

TEM sample preparation

TEM images were taken by negative staining technique. The samples were loaded onto carbon-coated grids (230-mesh copper grids that

had been coated with continuous thick carbon film) to cover the grid surface. Then, the grid was rinsed three times with ddH_2O. Carefully, water was allowed to move away from grid and then touch the edge of grid to filter paper sliver. The grid was then stained by 3% uranyl acetate stain solution for another three times, similar to the rinsing steps. After touching the stain solution, the grid was dried for a few minutes, and then, extra stain solution was absorbed using filter paper sliver. After rinsing and staining three times, copper grids with the sample covered were dried in air.

CD spectrum

Four different samples were prepared for CD analysis, including 0.75 wt % of N-pepABS hydrogels at pH 5.0 or pH 7.0, and diluted in N-pepABS solutions (0.01 wt %) and in methanol (0.005 wt %) at pH 9.0. Then, they were analyzed using JASCO J-1500 in 1-mm quartz cuvette. With a bandwidth set to 2 nm and a scanning speed set to 200 nm/min, all spectra have been collected in an average of three scans. The parameter of high tension value was kept between 200 and 650 during all measurements.

Analysis of intra-/extracellular accumulations of N-pepABS nanofibers

After different treatments with MDA-MB-231 cells, cell lysates and membrane residues were separated and then extracted with 1.2 ml of a mixture of methanol and ddH_2O (5:1). Standard samples of N-pepABS with concentrations of 1, 2, 5, 10, 20, and 50 μM were prepared to gain calibration curve. Each sample was analyzed by LC20AT UHPLC (Shimadzu Corporation, Japan), with gradient elution of H_2O and acetonitrile (0.1% TFA) as a mobile phase. The elution was programmed as follows: 0 to 20 min, 60 to 100%; flow rate was 1 ml/min, and the injection volume was 10 μl.

Cell cultures

MDA-MB-231 cells were cultured with Dulbecco's modified Eagle's medium containing 10% fetal bovine serum (FBS) and 1% penicillin-streptomycin in a CO_2 incubator at 37°C. For hypoxia experiments, MDA-MB-231 cells were cultured at 37°C in a hypoxic incubator with 1% O_2 and 5% CO_2. Before being treated with N-pepABS, MDA-MB-231 cells were precultured in the hypoxic incubator for about 12 hours.

CCK-8 assay

About 1×10^4 cells were seeded into each well of 96-well plate and treated with different doses of ABS, N-pepABS, N-pep, and pepABS for 72 hours. After each sample was incubated with CCK-8 agent for about 1 hour, cell viability was assessed through detecting the absorption at 450 nm with the exclusion at 600 nm.

Western blots

Cells were harvested, washed twice, and then resuspended with lysis buffer. After being denatured with SDS loading buffer by heating, equal amount of protein sample was uploaded and separated with SDS–polyacrylamide gel electrophoresis (PAGE). Then, the proteins were transferred from a PAGE to the polyvinylidene difluoride membrane. After being blocked with 5% fat-free milk, membranes were incubated with primary antibodies at 4°C overnight. The second day, membranes were washed three times with Tris-Buffered Saline Tween-20 and then incubated with horseradish peroxidase–conjugated secondary antibodies at room temperature for about 2 hours. After a second round of washes, membranes were treated with enhanced chemiluminescence reaction buffer, and each band was visualized.

Immunofluorescence

Cells were grown on the surface of glasses and treated with drug materials for the indicated time. Before incubation with primary antibodies at 4°C overnight, cells were fixed with 4% paraformaldehyde, treated with 0.1% Triton X-100, and blocked with 2% bovine serum albumin (BSA). After being washed with phosphate-buffered saline (PBS), each sample was incubated with secondary antibodies at room temperature for about 2 hours. After that, each sample underwent a second round of washes and was treated with 4′,6-diamidino-2-phenylindole staining buffer for about 5 min. Last, slides were washed and mounted with the antifade medium immediately.

Transwell assay

After being treated with drug materials for 24 hours under hypoxia condition (1.0% O_2), 4×10^4 cells were collected with serum-free medium containing 0.2% BSA and seeded into upper chamber, while the lower chamber was filled with 600 μl of medium containing 2.5% FBS. After that, cells migrated for about 10 hours and washed twice with ice-cold PBS. Before being imaged and calculated, cells on the lower surface of the film were fixed, washed, and stained with 0.1% crystal violet, while cells on the upper surface were cleared. The Transwell plate (3422) was obtained from Corning.

Transfections

Cells were grown in six-well plates for about 12 hours before transfection experiments were carried out. After small interfering RNA (siRNA) and transfection reagent were mixed well in Opti-MEM, cells were transfected with this mixture for about 6 hours. Then, Opti-MEM was replaced with complete medium. Being cultured overnight, cells were exposed to different treatments. Lipofectamine 2000 transfection reagent was purchased from Thermo Fisher Scientific, while siRNA sequence (5′-GGAAGAAAUCGCUGAGGAA-3′) and its negative control were from GenePharma.

SEM images for treated cancer cells

About 3×10^5 cells were grown on the glasses of each well at 37°C overnight and then precultured in a hypoxic incubator for about 12 hours at 37°C. After being treated with drug materials for the indicated time under hypoxia condition, cells were washed orderly with ice-cold PBS and distilled H_2O quickly, immersed into liquid nitrogen, and transferred into a freeze dryer immediately. After being dried overnight, each glass was coated with gold at 2 nm thick and then visualized.

TEM images for treated cancer cells

Cells of each sample were collected, washed twice, and fixed with 2.5% glutaraldehyde at 4°C overnight. After being washed with PBS, cells were fixed with 1% osmic acid, underwent a second round of washes, and dehydrated with gradient alcohol. Before being embedded, each sample was treated with a mixture of acetone and embedding medium, in which concentration was gradually elevated. Then, the sample was sliced to several pieces, stained with uranyl acetate and lead citrate orderly, and imaged.

Flow cytometry

Cells of each treatment were incubated with 2.5 μM lysosensor for 40 min at 37°C. After cells were collected and washed, the

intensity of lysosensor in each cell was detected with Accuri C6 flow cytometry.

Real-time polymerase chain reaction

Total mRNA was extracted with TRIzol agent (Invitrogen) according to the manufacturer's instructions. Equal amount of RNA was reverse-transcribed to complementary DNA (cDNA) through mixing with Moloney Murine Leukemia Virus reverse transcriptase, deoxynucleoside triphosphate (dNTP), and oligo(dT) according to the protocol from the manufacturer. After that, polymerase chain reaction process was carried out through mixing primers, cDNA, dNTP, and DNA polymerase, while the primers were synthetized by Sangon.

Animal experiments

Animal model was built up and analyzed depending on Institutional Animal Use and Care Committee at Chinese Academy of Sciences. About 4- to 6-week-old female nude mouse was injected with cancer cells subcutaneously. After the tumors were detectable, the mice were divided into some groups randomly, which was depending on the tumor volume (length × width^2/2) of each mouse. Then, the xenografts were treated by different chemicals, PBS or Dox. After being treated for several days, the mice were euthanized, while each organ or tumor was collected for further analysis.

Statistical analysis

A two-tailed *t* test was carried out to compare the statistical difference between two groups, while one-way analysis of variance (ANOVA) was used to compare multiple group differences. If the data were not suitable for the statistical analysis that had been listed above, then nonparametric tests were used. The bar graph was represented as means ± SD, and $^*P < 0.05$ was considered as statistically significant.

SUPPLEMENTARY MATERIALS

Supplementary material for this article is available at http://advances.sciencemag.org/cgi/content/full/5/9/eaax0937/DC1

Fig. S1. Hydrogel performances and characterizations of N-pepABS.
Fig. S2. CA IX–related cell behaviors in MDA-MB-231 and HeLa cells.
Fig. S3. CA IX–related endocytosis performances in MDA-MB-231.
Fig. S4. CA IX down-regulation inhibits nanofiber endocytosis under hypoxia.
Fig. S5. Acid vesicle injuries blocked protective autophagy in MDA-MB-231 cells.
Fig. S6. The antihypoxic cancer cells effects of N-pepABS treatment in vivo.
Fig. S7. Inhibition of tumor growth and metastasis on 4T1 tumor model.
Fig. S8. In vivo toxicity evaluation after different treatments.
Fig. S9. The synthesis and characterization of samples.

REFERENCES AND NOTES

1. J. M. Brown, A. J. Giaccia, The unique physiology of solid tumors: Opportunities (and problems) for cancer therapy. *Cancer Res.* **58**, 1408–1416 (1998).
2. P. Subarsky, R. P. Hill, The hypoxic tumour microenvironment and metastatic progression. *Clin. Exp. Metastasis* **20**, 237–250 (2003).
3. R. Carlisle, C.-C. Coussios, Mechanical approaches to oncological drug delivery. *Ther. Deliv.* **4**, 1213–1215 (2013).
4. W. R. Wilson, M. P. Hay, Targeting hypoxia in cancer therapy. *Nat. Rev. Cancer* **11**, 393–410 (2011).
5. C. T. Supuran, J.-Y. Winum, Carbonic anhydrase IX inhibitors in cancer therapy: An update. *Future Med. Chem.* **7**, 1407–1414 (2015).
6. R. A. Gatenby, K. Smallbone, P. K. Maini, F. Rose, J. Averill, R. B. Nagle, L. Worrall, R. J. Gillies, Cellular adaptations to hypoxia and acidosis during somatic evolution of breast cancer. *Br. J. Cancer* **97**, 646–653 (2007).
7. D. Neri, C. T. Supuran, Interfering with pH regulation in tumours as a therapeutic strategy. *Nat. Rev. Drug Discov.* **10**, 767–777 (2011).
8. E. Bourseau-Guilmain, J. A. Menard, E. Lindqvist, V. Indira Chandran, H. C. Christianson, M. Cerezo Magaña, J. Lidfeldt, G. Marko-Varga, C. Welinder, M. Belting, Hypoxia regulates global membrane protein endocytosis through caveolin-1 in cancer cells. *Nat. Commun.* **7**, 11371 (2016).
9. C. Ward, J. Meehan, P. Mullen, C. Supuran, J. M. Dixon, J. S. Thomas, J.-Y. Winum, P. Lambin, L. Dubois, N.-K. Pavathaneni, E. J. Jarman, L. Renshaw, I. Um, C. Kay, D. J. Harrison, I. H. Kunkler, S. P. Langdon, Evaluation of carbonic anhydrase IX as a therapeutic target for inhibition of breast cancer invasion and metastasis using a series of in vitro breast cancer models. *Oncotarget* **6**, 24856–24870 (2015).
10. J.-Y. Winum, F. Carta, C. Ward, P. Mullen, D. Harrison, S. P. Langdon, A. Cecchi, A. Scozzafava, I. Kunkler, C. T. Supuran, Ureido-substituted sulfamates show potent carbonic anhydrase IX inhibitory and antiproliferative activities against breast cancer cell lines. *Bioorg. Med. Chem. Lett.* **22**, 4681–4685 (2012).
11. R. G. Gieling, M. Babur, L. Mamnani, N. Burrows, B. A. Telfer, F. Carta, J.-Y. Winum, A. Scozzafava, C. T. Supuran, K. J. Williams, Antimetastatic effect of sulfamate carbonic anhydrase IX inhibitors in breast carcinoma xenografts. *J. Med. Chem.* **55**, 5591–5600 (2012).
12. H. S. Jung, J. Han, H. Shi, S. Koo, H. Singh, H.-J. Kim, J. L. Sessler, Y. L. Jin, J.-H. Kim, J. S. Kim, Overcoming the limits of hypoxia in photodynamic therapy: A carbonic anhydrase IX-targeted approach. *J. Am. Chem. Soc.* **139**, 7595–7602 (2017).
13. P. C. Mcdonald, J.-Y. Winum, C. T. Supuran, S. Dedhar, Recent developments in targeting carbonic anhydrase IX for cancer therapeutics. *Oncotarget* **3**, 84–97 (2012).
14. C. T. Supuran, Structure-based drug discovery of carbonic anhydrase inhibitors. *J. Enzyme Inhib. Med. Chem.* **27**, 759–772 (2012).
15. T. Dvir, B. P. Timko, D. S. Kohane, R. Langer, Nanotechnological strategies for engineering complex tissues. *Nat. Nanotechnology* **6**, 13–22 (2011).
16. C. Huang, Y. Zhang, H. Yuan, H. Gao, S. Zhang, Role of nanoparticle geometry in endocytosis: Laying down to stand up. *Nano Lett.* **13**, 4546–4550 (2013).
17. M. Stiti, A. Cecchi, M. Rami, M. Abdaoui, V. Barragan-Montero, A. Scozzafava, Y. Guari, J.-Y. Winum, C. T. Supuran, Carbonic anhydrase inhibitor coated gold nanoparticles selectively inhibit the tumor-associated isoform IX over the cytosolic isozymes I and II. *J. Am. Chem. Soc.* **130**, 16130–16131 (2008).
18. F. Ratto, E. Witort, F. Tatini, S. Centi, L. Lazzeri, F. Carta, M. Lulli, D. Vullo, F. Fusi, C. T. Supuran, A. Scozzafava, S. Capaccioli, R. Pini, Plasmonic particles that hit hypoxic cells. *Adv. Funct. Mater.* **25**, 316–323 (2015).
19. L. A. Estroff, A. D. Hamilton, Water gelation by small organic molecules. *Chem. Rev.* **104**, 1201–1218 (2004).
20. J. Boekhoven, S. I. Stupp, 25th anniversary article: Supramolecular materials for regenerative medicine. *Adv. Mater.* **26**, 1642–1659 (2014).
21. D. J. Smith, G. A. Brat, S. H. Medina, D. Tong, Y. Huang, J. Grahammer, G. J. Furtmüller, B. C. Oh, K. J. Nagy-Smith, P. Walczak, G. Brandacher, J. P. Schneider, A multiphase transitioning peptide hydrogel for suturing ultrasmall vessels. *Nat. Nanotechnol.* **11**, 95–102 (2016).
22. C. Yan, M. E. Mackay, K. Czymmek, R. P. Nagarkar, J. P. Schneider, D. J. Pochan, Injectable solid peptide hydrogel as a cell carrier: Effects of shear flow on hydrogels and cell payload. *Langmuir* **28**, 6076–6087 (2012).
23. H. Wang, Z. Feng, B. Xu, Bioinspired assembly of small molecules in cell milieu. *Chem. Soc. Rev.* **46**, 2421–2436 (2017).
24. K. Han, J. Zhang, W. Zhang, S. Wang, L. Xu, C. Zhang, X. Zhang, H. Han, Tumor-triggered geometrical shape switch of chimeric peptide for enhanced in vivo tumor internalization and photodynamic therapy. *ACS Nano* **11**, 3178–3188 (2017).
25. S. H. Medina, S. E. Miller, A. I. Keim, A. P. Gorka, M. J. Schnermann, J. P. Schneider, An intrinsically disordered peptide facilitates non-endosomal cell entry. *Angew. Chem. Int. Ed. Engl.* **55**, 3369–3372 (2016).
26. Z. Zheng, P. Chen, M. Xie, C. Wu, Y. Luo, W. Wang, J. Jiang, G. Liang, Cell environment-differentiated self-assembly of nanofibers. *J. Am. Chem. Soc.* **138**, 11128–11131 (2016).
27. M. T. Jeena, L. Palanikumar, E. M. Go, I. Kim, M. G. Kang, S. Lee, S. Park, H. Choi, C. Kim, S.-M. Jin, S. C. Bae, H. W. Rhee, E. Lee, S. K. Kwak, J.-H. Ryu, Mitochondria localization induced self-assembly of peptide amphiphiles for cellular dysfunction. *Nat. Commun.* **8**, 26 (2017).
28. T. Ji, Y. Zhao, Y. Ding, J. Wang, R. Zhao, J. Lang, H. Qin, X. Liu, J. Shi, N. Tao, Z. Qin, G. Nie, Y. Zhao, Transformable peptide nanocarriers for expeditious drug release and effective cancer therapy via cancer-associated fibroblast activation. *Angew. Chem. Int. Ed. Engl.* **55**, 1050–1055 (2016).
29. Y. Kuang, J. Shi, J. Li, D. Yuan, K. A. Alberti, Q. Xu, B. Xu, Pericellular hydrogel/nanonets inhibit cancer cells. *Angew. Chem. Int. Ed. Engl.* **53**, 8104–8107 (2014).
30. P.-P. Yang, Q. Luo, G.-B. Qi, Y.-J. Gao, B.-N. Li, J.-P. Zhang, L. Wang, H. Wang, Host materials transformable in tumor microenvironment for homing theranostics. *Adv. Mater.* **29**, 1605869 (2017).
31. H. Wang, Y. Wang, A. Han, Y. Cai, N. Xiao, L. Wang, D. Ding, Z. Yang, Cellular membrane enrichment of self-assembling D-peptides for cell surface engineering. *ACS Appl. Mater. Interfaces* **6**, 9815–9821 (2014).
32. T. B. Potocky, A. K. Menon, S. H. Gellman, Effects of conformational stability and geometry of guanidinium display on cell entry by β-peptides. *J. Am. Chem. Soc.* **127**, 3686–3687 (2005).
33. L. L. Lock, C. D. Reyes, P. Zhang, H. Cui, Tuning cellular uptake of molecular probes by rational design of their assembly into supramolecular nanoprobes. *J. Am. Chem. Soc.* **138**, 3533–3540 (2016).
34. J. Yang, K. Koruza, Z. Fisher, W. Knecht, L. Baltzer, Improved molecular recognition of carbonic anhydrase IX by polypeptide conjugation to acetazolamide. *Bioorg. Med. Chem.* **25**, 5838–5848 (2017).

35. M. Ceruso, M. Bragagni, Z. Alothman, S. M. Osman, C. T. Supuran, New series of sulfonamides containing amino acid moiety act as effective and selective inhibitors of tumor-associated carbonic anhydrase XII. *J. Enzyme Inhib. Med. Chem.* **30**, 430–434 (2014).
36. J. Li, Y. Kuang, Y. Gao, X. Du, J. Shi, B. Xu, D-amino acids boost the selectivity and confer supramolecular hydrogels of a nonsteroidal anti-inflammatory drug (NSAID). *J. Am. Chem. Soc.* **135**, 542–545 (2012).
37. M. Zatovičová, S. Pastoreková, Modulation of cell surface density of carbonic anhydrase IX by shedding of the ectodomain and endocytosis. *Acta Virol.* **57**, 257–264 (2013).
38. G. Liu, J. Sheng, H. Wu, C. Yang, G. Yang, Y. Li, R. Ganguly, L. Zhu, Y. Zhao, Controlling supramolecular chirality of two-component hydrogels by *J*- and *H*-aggregation of building blocks. *J. Am. Chem. Soc.* **140**, 6467–6473 (2018).
39. Y. Deng, W. Yuan, Z. Jia, G. Liu, H- and J-aggregation of fluorene-based chromophores. *J. Phys. Chem. B* **118**, 14536–14545 (2014).
40. Z. Sun, Z. Li, Y. He, R. Shen, L. Deng, M. Yang, Y. Liang, Y. Zhang, Ferrocenoyl phenylalanine: A new strategy toward supramolecular hydrogels with multistimuli responsive properties. *J. Am. Chem. Soc.* **135**, 13379–13386 (2013).
41. C. F. Thorn, C. Oshiro, S. Marsh, T. Hernandez-Boussard, H. McLeod, T. E. Klein, R. B. Altman, Doxorubicin pathways: Pharmacodynamics and adverse effects. *Pharmacogenet. Genomics* **21**, 440–446 (2011).
42. J. Huang, T. Zhang, K. Ma, P. Fan, Y. Liu, C. Weng, G. Fan, Q. Duan, X. Zhu, Clinical evaluation of targeted arterial perfusion of verapamil and chemotherapeutic drugs in interventional therapy of advanced lung cancer. *Cancer Chemother. Pharmacol.* **72**, 889–896 (2013).
43. Y.-M. Liu, H. Qin, C.-B. Wang, X.-H. Fang, Q.-Y. Ma, Comparison of therapeutic effectiveness of combined interventional therapy for 1126 cases of primary liver cancer. *World J. Gastroenterol.* **12**, 5060–5063 (2006).

Acknowledgments: We thank S. Bai (Institute of Process Engineering, Chinese Academy of Sciences) for providing the rheology data. **Funding:** The work reported here is financially supported by the National Natural Science Foundation of China (31571022 and 31871004), the National Basic Research Program of China (2016YFA0201600 and 2016YFA0203204), Key Program for International S&T Cooperation Projects of China (2016YFE0133100), the Science Fund for Creative Research Groups of the National Natural Science Foundation of China (11621505), CAS Key Research Program for Frontier Sciences (QYZDJ-SSW-SLH022), Bureau of International Co-operation Chinese Academy of Sciences (GJHG1852), the National Science Fund for Distinguished Young Scholars (11425520), and the National Science Fund for Excellent Young Scholars (31622026). **Author contributions:** J.L., K.S., and C.C. conceived and designed experiments. K.S., Z.F.S., and J.L. performed experiments. K.S. and J.L. collected and analyzed data. W.F., M.X., S.X., T.L., M.Y., M.C., and H.Z. took part in animal experiments. Y.L., B.H., and X.C. took part in discussions. C.C. supervised the project. J.L., K.S., and C.C. wrote the manuscript. All authors discussed the results and commented on the manuscript. **Competing interests:** The authors declare that they have no competing interests. **Data and materials availability:** All data needed to evaluate the conclusions in the paper are present in the paper and/or the Supplementary Materials. Additional data related to this paper may be requested from the authors.

Submitted 21 February 2019
Accepted 6 August 2019
Published 6 September 2019
10.1126/sciadv.aax0937

Citation: J. Li, K. Shi, Z. F. Sabet, W. Fu, H. Zhou, S. Xu, T. Liu, M. You, M. Cao, M. Xu, X. Cui, B. Hu, Y. Liu, C. Chen, New power of self-assembling carbonic anhydrase inhibitor: Short peptide–constructed nanofibers inspire hypoxic cancer therapy. *Sci. Adv.* **5**, eaax0937 (2019).